Gold nanocups with multimodal plasmon resonance for quantum-dot random lasing

Jian Zhang^{a,b}, Zhiwei Li^b, Yaocai Bai^b, Yadong Yin^{b,*}

ARTICLE INFO

Article history:

Received

Received in revised

Accepted

Keywords:

Gold nanocups

Ripening

Seeded growth

Multimodal plasmon resonance

Quantum dot random laser

ABSTRACT

Reduction of symmetry in plasmonic nanostructures may lead to great opportunities in controlling their photophysics of extinction, local field, light response, and plasmonic interactions. With their strong light scattering and unique modulation of field distribution, plasmonic nanocups hold great potential for applications in random laser, threedimensional optical nanoantenna, and optical coherence tomography imaging. Here we demonstrate a novel and robust solution-phase synthesis approach to gold nanocups, which combines templating and seeded growth techniques to precisely control the size, morphology, and composition of the nanocups. Ripening is the key strategy in this wet-chemistry process to ensure primary anisotropic growth of gold within the cup-shaped space provided by each template, consisting of a silica nanosphere and a flexible resorcinol-formaldehyde resin shell. The resulting plasmonic nanocups possess three types of plasmon resonance modes, including axial, transverse S, and transverse P modes, determined by the polarization of the incident light. This robust and scalable synthesis allows the production of gold nanocups with high quality and efficiency, opening the door to unique photophysical properties and many potential applications, as demonstrated by their excellent performance in plasmonic quantum dot random lasing.

1. Introduction

Controlling the shape, size, and composition of metal nanostructures allows for tailoring the wavelength of their localized surface plasmon resonance (LSPR), local field distribution, absorption and scattering properties [1]. Particularly shaped metal nanoparticles or those with spatial arrangements may exhibit a variety of unique optical properties,

enabling many applications such as light bending [2], directional light scattering [3-5], negative refraction [6, 7], superlens [8], metalens [9], optical cloaking [10], zero refraction [11], and magnetic plasmon resonance [12-14]. Compared with nanospheres, anisotropic metal nanoparticles such as gold nanorods show unique plasmonic properties, which are tunable by controlling the aspect ratio, orientation, shape, and composition [15-17]. Similarly, plasmonic nanocups (also known as semishells) with unique plasmon resonance modes have rich photophysical properties that may enable numerous attractive optical devices. For example,

^a Key Laboratory of the Ministry of Education for Optoelectronic Measurement Technology and Instrument, Beijing Information Science & Technology University, Beijing, 100192, China

^b Department of Chemistry, Center for Catalysis, University of California Riverside, Riverside, California 92521, United States

^{*} Corresponding authors. Email address: yadong.yin@ucr.edu

gold (Au) nanocups can redirect incident light to the opening direction owing to the magnetic dipole plasmon resonance, which has been used for threedimensional optical nanoantennae [2, 3, 4, 18]. Their strong light scattering and high chemical stability also make them efficient contrast agents for enhancing optical coherence tomography (OCT) imaging in biological tissues [19]. By simply controlling their thickness, one can optimize their thermal conversion efficiency and light scattering characteristics for highly efficient cancer multimodal imaging and photothermal therapy [20]. The transverse P resonance mode can generate strong electric fields localized around the nanocup edges to benefit surface-enhanced Raman scattering (SERS) [21, 22] and allow three-dimensional, high-efficiency generation of second harmonic light [23, 24].

These compelling applications and photophysical investigations require precise control over the morphology and spectral response of the metal nanocups. Reliable fabrication approaches are therefore highly desirable, which include physical and wet-chemistry routes [25]. The physical preparation method can produce plasmonic nanocups with various compositions or collective orientations [2, 22, 25-29]. However, their obvious disadvantages, including low yield, complicated preparation process and high cost, hinder their practical applications in biomedicine and optical devices. Wet-chemistry methods have been reported using PdS and SiO₂ as the templates to synthesize gold nanocups [19, 21]. By performing vertex-initiated selective overgrowth of Au on PbS octahedral nanoparticles, it is possible to produce gold nanocups

with different opening sizes. This method is difficult to achieve hemispherical shell-type gold nanocups with uniform thickness, limiting their optical applications such as optical nanoantenna. In another method, we used template-assisted hightemperature calcination to obtain Au nanocups with excellent morphology, which, however, involves multi-step liquid-phase reaction and solid-state processing [19]. Here, we demonstrate a new wetchemistry synthesis method to prepare high-quality gold nanocups with precisely tunable opening, size, and plasmonic properties. Three types of plasmon resonance modes (axial, transverse S, and transverse P modes) are found in gold nanocups of different sizes, which are further confirmed by simulation of their extinction spectra, electric field, and charge distribution. By taking advantage of the nanocups' strong scattering properties, we further develop a quantum dot random laser by simply mixing CdSe quantum dots with gold nanocups, demonstrating excellent optical feedback of Au nanocups with the full width at half maxima (FWHM) of 4 nm. This unique space-confined seeded growth method has compelling advantages of large-scale production, easy morphology control, and high reproducibility. It can be extended to producing nanocups of different chemical components by simply changing metal precursors, setting the stage for fully exploiting their attractive optical properties and emerging practical applications.

2. Experimental Section

2.1. Synthesis of SiO2 nanospheres

A modified Stöber method was used to prepare colloidal silica nanospheres [30, 31]. For 290-nm

silica nanospheres, 24.75-mL water, 26.25-mL ethanol, and 9-mL aqueous ammonia (28%) were firstly mixed. Then, 4.5 mL of tetraethyl orthosilicate (TEOS) and 35.5 mL of ethanol were mixed for 30 seconds and then added into the first solution. After stirring for 2 hours at room temperature, the silica nanospheres were collected by centrifugation and washed with ethanol (2 times) and water (1 time), which was re-dispersed in 20 mL of water. For silica nanosphere around 110 nm, 98 mL of ethanol, 10 mL of water, 1.25 mL of aqueous ammonia (28%) and 5 mL TEOS were mixed under stirring for 16 hours at room temperature. The product was then collected by centrifugation and washed by ethanol (2 times) and water (1 time), finally dispersed in 20 mL of water. For silica nanosphere around 200 nm, 23 mL of ethanol, 4 mL of water, 0.86 mL of TEOS were mixed first under stirring for 3 mins. Then, 0.65 mL of aqueous ammonia (28%) was added, and the reaction was stirred for 4 hours. The silica spheres were washed by ethanol and water, and then dispersed in 20 mL of water.

2.2. Modified silica nanospheres with APTES

The SiO₂ nanoparticles are further modified by 3-aminopropyltriethoxysilane (APTES) to enable the attachment of Au seeds. Typically, 5 mL of silica sphere aqueous solution was washed three times with ethanol and was dispersed in 20 mL of ethanol. Then 3 mL of APTES was added to the solution under ultrasonication. The solution was then heated at 78 °C for 3 hours and stirred at room temperature for 24 hours to ensure sufficient modification of APTES to the silica nanoparticle surface. After the reaction, the mixture was washed with

ethanol three times and water two times, and the final product was dispersed in 20 mL of water.

2.3. Synthesis of THPC-capped gold seeds

An aqueous solution was prepared by mixing 95.5 mL of water, 315 μ L of NaOH (2M), 126 μ L of tetrakis(hydroxymethyl)phosphonium chloride (THPC) (20 %). With stirring at 800 rpm, 290 μ L of 0.25 M HAuCl₄ was added to the mixed solution. After stirring 5 minutes, the solution was placed in the refrigerator and aged for 2 weeks at 4 °C.

2.4. Synthesis of SiO₂@Au Nanospheres

6 mL of gold seed solution and 3 mL of APTES-modified silica nanoparticles were added into a 50-mL plastic tube and then sonicated for half an hour. Excess Au seeds were removed by washing the mixture one time using deionized (DI) water and further dispersed in 10 mL of DI water. In facilitating coating resorcinol-formaldehyde (RF) resin, 3 mL of PVP aqueous solution (mass ratio of 5%) was added into the above seed solution, and the mixture was magnetically stirred for 6-8 hours. And excess PVP was removed by washing one time. The PVP-modified nanoparticles were dispersed in 20 mL of DI water.

2.5. Synthesis of SiO₂@Au@RF Nanospheres

A solution was prepared by mixing 5 mL of the above silica@gold nanosphere solution and 23 mL of water, to which 22.5 ml of formaldehyde (F), 31.5 mg of resorcinol (R), and 50 μ L of ammonia solution (2.8%) were added in sequence. The reaction was kept at 50 °C for 2 hours and then at 100 °C for a few hours. During the later high-tempera-

ture condensation, the RF nanoshells became stable. Another interesting effect of this process is the slight etching of silica nanosphere surfaces, leading to a small gap between the core and the RF shell. The RF thickness is approximately 30 nm.

2.6. Synthesis of Au nanocups

To grow 290-nm Au nanocups in a controllable manner, 200 μ L of 5 wt% PVP aqueous solution, 290 μ L of 0.2 M potassium iodide (KI) aqueous solution, 290 μ L of 0.1 M ascorbic acid (AA) solution, 45 μ L of 0.25 M HAuCl₄ solution, and 20 μ L of SiO₂@Au@RF solution were added into 2 mL of milli-Q water in sequence. After 20 minutes, the final products were washed three times by water and dispersed in 1mL of water.

For 200-nm Au nanocups, 200 μL of 5 wt% PVP aqueous solution, 120 μL of 0.2 M KI solution, 120 μL of 0.1 M AA solution, 18 μL of 0.25 M HAuCl₄ solution, and 7.5 μL of SiO₂@Au@RF seed solution were added into 2 mL of Milli-Q water. After 20 minutes, the mixture was washed 3 times with deionized water and dispersed in 1 mL of water to obtain SiO₂@Au nanocup@RF nanospheres.

2.7. Etching SiO₂ and RF to release Au nanocups

To remove the SiO₂ and RF, we added 15 mL of 2M NaOH solution into the SiO₂@Au@RF nanosphere solution, stirred for 12 hours at 60 °C. The gold nanocups were obtained after being washed twice with deionized water.

2.8. Simulation

All optical spectra and near-field distribution were performed using FDTD Solutions 2020a (Lumerical Solutions). During simulation, total-field scattered-field (TFSF) was selected as the light source with a range of 400-2000 nm to illuminate the gold nanocup under different incident directions and polarization modes, and the amplitude is set to 1. The surrounding refractive index of the gold nanocup is set to 1.33 for water, which is consistent with the experiment. The size of the gold nanocup in the simulation is consistent with the SEM and TEM images in the experiment. Johnson and Christy's optical constants were used for gold. The mesh of nanocup and its surrounding is divided into 1 nm in size.

2.9. Fabrication of quantum dot random laser

The gold nanocup is synthesized in the water phase and needs to be transferred to the oil phase to mix with the quantum dot solution. 2 mL of octanethiol was added to 10 mL of absolute ethanol, which was sonicated for 4 minutes to form a mixed solution. The gold nanocup aqueous solution was centrifuged to remove water. The obtained Au nanocups were dried and then dispersed in a 1.5 mL mixture of ethanol and octanethiol. The mixture was shaken for 8 hours and dried in a fume hood. Then, xylene was added into a centrifuge tube, and the gold nanocup solution was prepared with a concentration of 3 mg/mL. The quantum dots were dispersed in xylene under different concentrations. The gold nanocup solutions and the quantum dot solutions were mixed and spin-coated on a quartz substrate to obtain laser devices.

2.10. Measuring quantum dot random laser

A femtosecond pulse laser with 400-nm wavelength, pulse duration of 200 fs, repetition rate of 1 kHz was used to vertically excite the sample. The diameter of the pulsed laser spot is about 3 mm. The receiving fiber was at an angle of approximately 45 degrees to the excitation light. A spectrometer (Maya 2000 Pro, Ocean Optics, Dunedin, FL, USA) with a spectral resolution of 0.4 nm was used to measure the laser emission spectra.

3. Results and Discussion

3.1. Design and fabrication of the plasmonic Au nanocups

The wet-chemistry synthesis method uses templated strategy to directly synthesize Au nanocups with highly tunable structures and plasmonic properties. Its key step is to introduce a proper space in which the seeded growth of Au produces complementary nanocups to the initial confined spaces. As outlined in Figure 1a, our synthetic approach uses SiO₂/Au@RF as colloidal templates. It involves the

attachment of Au seeds on monodisperse silica nanospheres of any chosen sizes through electrostatic interactions and surface coating of permeable and deformable resorcinol-formaldehyde (RF) resin. The following etching of the silica surface in an alkaline solution is important because it provides empty spaces between silica and RF, facilitating the ripening of small seeds during the growth. The deformable RF shells offer enough space for the continuous deposition of Au atoms and, more importantly, regulate the particle growth into exquisite nanocups. Finally, gold nanocups are obtained by removing the templates through chemical etching. This seeded growth approach is simple but provides elegant control over the nanocup diameter, thickness, and opening size. While the silica nanospheres determine the diameter of the nanocups, the gap size and the RF thickness control the nanocup thickness. Besides, the opening size of Au nanocups can be readily tuned during the seeded growth process.

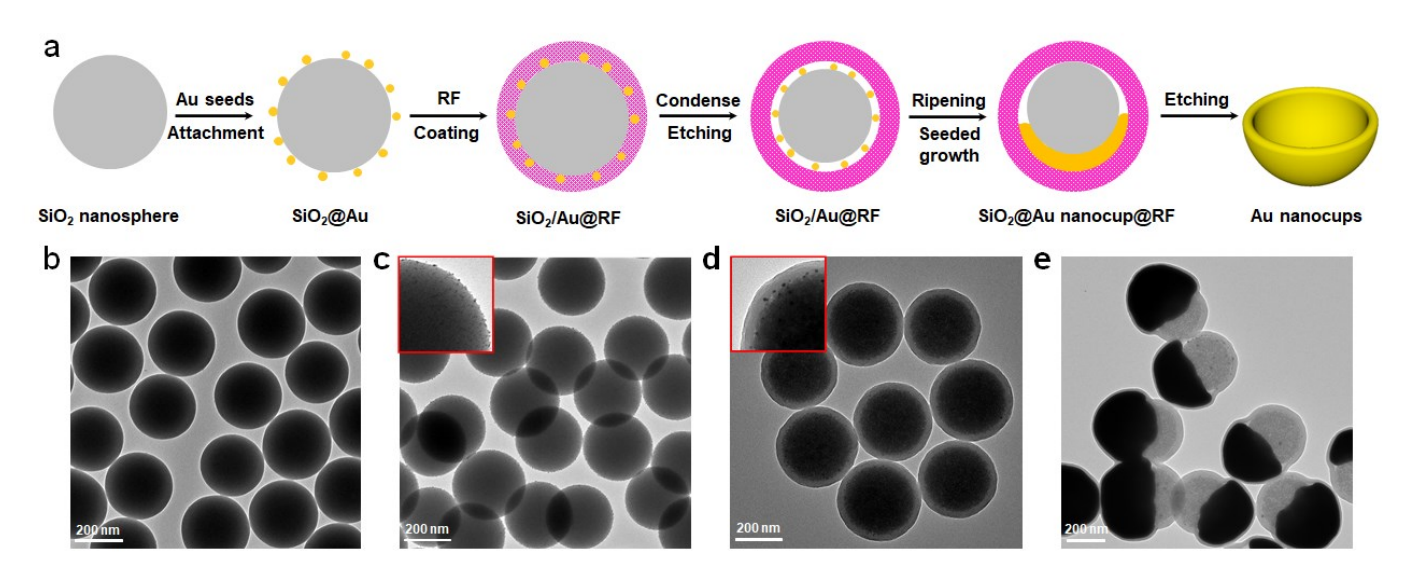


Fig. 1 (a) Schematic illustration of the space-confined seeded growth of gold nanocups. TEM images of (b) SiO₂ nanospheres, (c) SiO₂/Au seeds nanospheres, (d) SiO₂/Au@RF nanospheres, (e) SiO₂@Au nanocup@RF nanospheres. The diameter of silica nanospheres is about 290 nm.

A modified sol-gel process is used to prepare monodisperse silica nanospheres of 290 nm (Fig. 1b) [31]. Then APTES is used to modify silica nanospheres so that they are positively charged

due to the presence of amino groups on the particle surface. Negatively charged Au seeds of ~2 nm can be absorbed through electrostatic interactions [32]. The TEM images in Figure 1c demonstrate the uniform attachment of Au seeds across the particle surfaces. Then RF coating was performed using a sol-gel method, which occurred at 50 °C for 2 hours [32, 33]. The obtained SiO₂/Au@RF nanospheres feature homogeneous Au seeds, on which the deposition of reduced Au atoms produces uniform Au shells due to the fusion of neighboring Au domains. This growth mode produces conformal Au coating on nanoparticles instead of defined nanocups. Therefore, introducing Ostwald ripening is essential for the growth of Au nanocups, which involves the oxidative dissolution of small Au seeds and reductive deposition on large ones. A remarkable consequence of the Ostwald ripening is the deposition of Au atoms on one seed within each template and the controllable growth of the particle into nanocups. To facilitate this chemical process, the SiO₂/Au@RF nanospheres are further treated at 100 °C for more than 1 hour to slightly etch the silica cores. It produces well-defined gaps at the interfaces where the exposed Au seeds will be susceptible to chemical etching. In addition, the gap size can be easily controlled by the reaction time, with long etching time leading to large gaps and thick Au nanocups. Meanwhile, the high temperature will further condense RF shells, making them mechanically flexible and chemically stable to confine the seeded growth of Au nanocups. The thickness of RF coating is ~30 nm as shown in Figure 1d. The formation of Au nanocups during

the seeded growth could be monitored by UV-Visible-NIR extinction spectra. As the seeded growth occurs, the gold seeds first ripen to single Au nanoparticle and then gradually grow into nanocups as the extinction peak has a gradual redshift and multiple plasmon modes appear (Fig.S1, Supporting Information). Notably, the continuous redshift of the plasmonic peaks implies the gradual growth of Au nanocups instead of nanoshells because the seeded growth of Au nanoshells features a slight blueshift when complete Au nanoshells form [34]. For the gold nanocups synthesized by templating against 290-nm silica and 30-nm RF shells, the nanocup thickness is about 50 nm (Fig.1e). The silica spheres and RF layers can be removed by NaOH solution (2M) at 60 °C for 12 hours, thus releasing the Au nanocups from the templates. As the gold nanoparticles grow, the RF is gradually stretched and thinned because of the seeded growth-induced volume expansion, which is interestingly evidenced by the thickness difference between RF layers on Au and layers on silica. In previous work, the RF was only used as a sacrificial layer [19]. Our interesting results demonstrate the critical role of RF shells in regulating the seeded growth of Au nanocups. While its high permeability allows dexterous confined growth, its deformability in response to Au deposition leads to well-defined nanocups. From Figure 1e, we can see that the gold nanocups have a uniform shape and smooth surface. The Janus nanostructures are evidenced by the clear contrast in nanocups with interesting lateral orientation. The success of this fabrication method should be attributed to two key steps. The first one is the condensation process, which produces tunable gaps and the deformable RF confining layers. The second one is the Ostwald ripening, which is crucial for obtaining nanocups.

3.2. Tunability of the plasmonic Au nanocups

This synthesis method can produce a set of Au nanostructures with different shapes by simply tuning the ratio between growth solution and seed solution. Specifically, tuning the ratio allows to precisely and systematically control the opening size, height, and thickness of the Au nanocups. As shown in Figures 2 (a)-(f), the shape of the nanoparticles gradually changed from nanocup to nanoshell if a seed solution of 35 µl, 30 µl, 25 µl, 20 μl, 10 μl, and 5 μl was used, with a constant volume of growth solution. In Figure 2a, the seeded growth on a large amount of Au seeds yields small Au nanostructures with an interesting cap-like shape. While the seeded growth of Au prefers spherical shapes as regulated by surface energy, the confinement of deformable RF shells limits its free growth along radial directions. This sequence of events creates shallow Au nanocups with their thickness gradually increasing from the cup edge to the center. This observation is also true for nanocups with different openings and diameters. As the seed concentration decreases in the growth solution, the final Au nanostructures become large due to more Au atom deposition on each template. It produces thick Au nanocups with a first increase (from Fig.2b to Fig.2d) and then decrease (from Fig.2d to Fig.2e) in the opening. These phenomena indicate simultaneous Au deposition along the cup radius and template edge spaces, which is favored by the surface energy of Au colloids and the confinement effect of RF shells, respectively. This competing effect produces thick nanocups, whose continuous growth along the silica-RF interfaces leads to the interesting dependence of nanocup openings on seed concentration. If seed concentration is further reduced, the overgrowth of Au nanocups yields compact Au nanoshells (Fig.2f). These observations imply that the Au nanoshells are eccentric due to the templating effect of silica cores. This simple method allows convenient control over the size and morphology of Au nanocups and, therefore, greatly facilitates a systematic study of their optical properties.

During the synthesis process, the size of the gap and the thickness of the RF layer significantly affect the morphology of the prepared gold nanoparticles. Figures S2(a-c) show the TEM images of gold nanoparticles prepared by etching silica in different duration. The diameter of initial silica nanospheres is about 233 nm, which is reduced to 224 nm, 219 nm, and 208 nm after being etched for 1 h, 2 h, and 3 h, respectively. From Figures S2(a-c), it can be concluded that Au nanocups with different sizes and thicknesses can be produced by using these templates. The thickness of the Au nanocups increases from 15 nm to 20 nm when prolonging the etching time from 2 hours to 3 hours. The thickness of the RF layer is another important factor in the successful growth of uniform Au nanocups. Figure S2(d-e) shows the TEM images of the gold nanoparticles obtained from 12-nm, 17.7-nm, and 29-nm RF shells. When the thickness of the RF layer is 12 nm, the fast diffusion of Au precursors through the thin shells leads to a quick reduction and Au deposition, which is expected to suppress the ripening process. One consequence of these events is the high likelihood that the seeded growth of Au occurs on multiple seeds inside the gap, leading to irregular shapes and large morphological variation among individual nanostructures (Fig.S2d). When the RF shells increase to 17.7 nm, we observed regular and uniform Au nanocups (Fig.S2e), suggesting an optimal condition for balancing ripening and growth kinetics. Further increasing RF shells to 29 nm, however, yields large free Au nanoparticles without noticeable seeded growth at the silica-RF interfaces largely because of the considerably slow diffuse and strong confinement of thick RF shells (Fig.S2f).

It is worth noting that the prepared gold nanocups are not perfect hemispherical shells, which instead have an increasing thickness from the nanocup edge to the bottom. This is because RF is flexible, and there is a competition between RF confinement and seeded growth, especially in the early growth stage. Although the radius growth is confined, continuous Au deposition is still possible via deforming RF shells, leading to thick Au nanocups, while the deposition at the gap edge produces large nanocups. Our experimental results demonstrate that the successful production of high-quality Au nanocups requires delicate control over the ripening and reduction kinetics, which can be readily tuned by changing RF thickness, gap size enabled by this unique synthetic method.

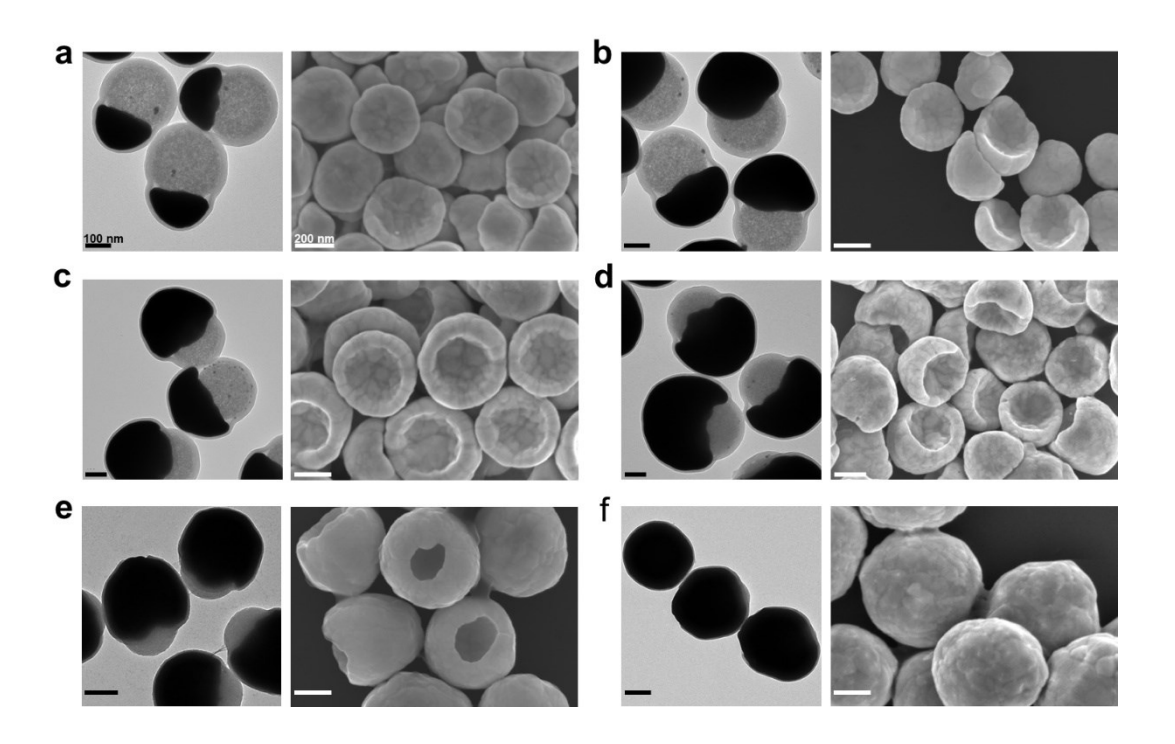


Fig. 2 TEM (left panels) and SEM (right panels) images of the Au nanoparticles prepared by gradually decreasing the amount of seed solution. (a-f) The amount of the seed solution is 35 μ l, 30 μ l, 25 μ l, 20 μ l, 10 μ l, and 5 μ l, respectively. All scale bars are 100 nm in the TEM images and 200 nm in the SEM images.

3.3. Photophysical properties of plasmonic nanocups

We experimentally and theoretically studied the photophysical properties of gold nanocups with different sizes in various incident light modes. The three-dimensional FDTD method was used to simulate the absorption, scattering, extinction spectra, map electric field distribution and charge distribution. The experimental and simulated results indicate that the gold nanocups have three types of plasmon resonance modes, which are denoted as axial, transverse S and transverse P modes and are defined according to the polarization of incident light. When the direction of the electric field is parallel and perpendicular to the axis of symmetry, the modes are defined as axial and transverse modes, respectively. To further clarify the transverse modes, the plane made of incident beam direction and the symmetry axis of Au nanocups is introduced as the incident plane. The transverse modes are further divided into transverse P and transverse S modes when the polarization of the incident light is parallel and perpendicular to the incident plane, respectively. All calculations use water as the external dielectric medium to be consistent with actual measurements.

Figure 3a shows the measured extinction spectra and the simulated spectra of Au nanocups with 95-nm inner radius, 130-nm outer radius, and 130-nm height, corresponding to the sample in Figure S2e. The experimental spectra of gold nanocup present three distinct extinction peaks at 1064 nm, 709 nm, and 601 nm. To confirm the plasmon resonance modes, we used the FDTD method to simu-

late the spectra, charge and electric field distribution. As shown in Figure 3a, the simulated extinction spectrum is in good agreement with the measured spectrum, which shows three resonance peaks, 1064 nm, 721 nm, and 612 nm. Obviously, the extinction mainly comes from scattering because scattering intensity is much higher than absorption. In Figure 3b, the axial mode has an extinction peak at 593 nm. In Figure 3c, the positive and negative charges are distributed axially along the gold nanocups. Correspondingly, strong electric fields are generated at the nanocup edges and bottoms.

The transverse S mode has three extinction peaks located at 619 nm, 721 nm, and 1081 nm (Fig.3d). In this excitation mode, we can treat the plasmon modes of the gold nanocup as the plasmon coupling between a gold hemisphere and a hemicavity. The charge distribution is similar to symmetric and asymmetric plasmon resonance modes of gold nanoshells [35]. The surface charge and electric field distribution in Figure 3e suggest dipolar, quadrupolar, and hexapolar resonance for LSPR peaks at 1081, 721 and 619 nm, respectively. Clearly, the electric fields at 1081, 721 and 619 nm exhibit asymmetrical distribution because of the mixing of the dipolar component and the multipolar component [36]. The LSPR exhibits narrower linewidth at 721 nm and 619 nm, with FWHM of ~60 nm and ~15 nm, respectively, and high quality factors (Q = $\lambda/\Delta\lambda$, Q=12 for the peak at 721 nm, Q=41 for the peak at 619 nm), which represents the subradiant mode (dark mode). The extinction profile at 1081 nm is broad (FWHM 280 nm, Q=4), indicating a superradiant mode (bright mode). The highorder plasmon resonance for transverse S mode and transverse P mode becomes more obvious as the size of the nanocup increases.

The transverse P modes in Figure 3f present two extinction peaks at about 1064 nm and 578 nm. Under 1064 nm excitation, the charge flows along the nanocup curve, and the inner and outer walls of the nanocup show the same charge distribution (Fig.3g). The nanocup edge produces a strong electric field distribution corresponding to the magnetic

resonance mode. It has been widely demonstrated that the strong electric fields at the nanocup edge have excellent SERS performance[21,22]. Under 578-nm light excitation, the charge of the outer interface edge is opposite to the inner interface, and the electric field distribution exhibits quadrupolar-like resonance mode. The scattering is much stronger than the absorption for all the resonance modes of Au nanocups, demonstrating the scattering-dominated optical properties.

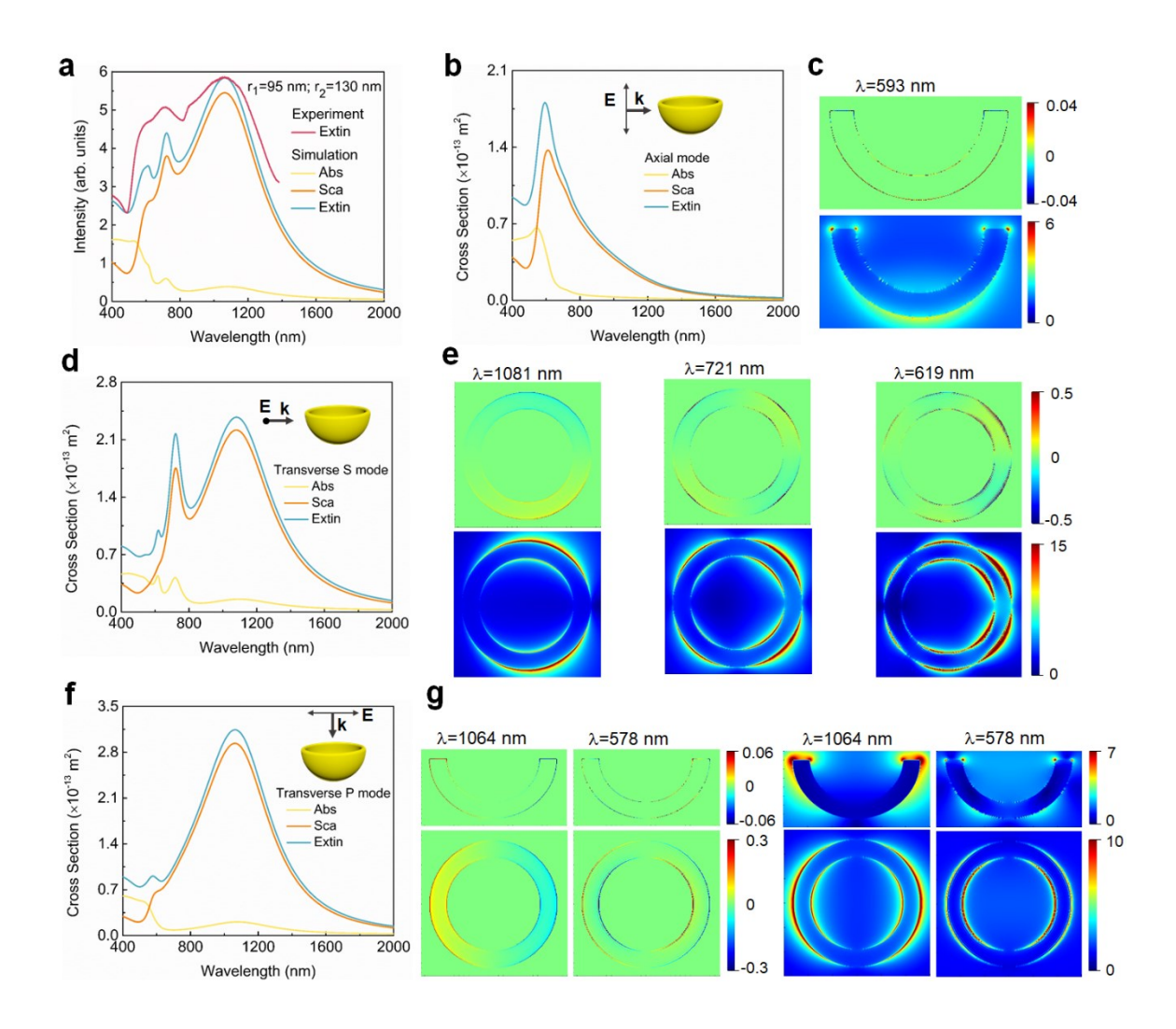


Fig. 3 Plasmonic properties of the Au nanocups with the inner radius of 95 nm and outer radius of 130 nm. (a) The experimental and the simulated spectra. (b) The simulated spectra of Au nanocups under axial mode. (c) The corresponding charge (top panel) and electric field distribution (bottom panel) at the resonant wavelength. (d) The simulated spectra under transverse S mode. (e) The corresponding charge (top panels) and electric field distribution (bottom panels) at different resonant wavelengths. (f) The simulated spectra under transverse P mode. (g) The corresponding charge (left panels) and electric field distribution (right panels) at different resonant wavelengths.

The size of the nanocup strongly influences its LSPR properties. In experiments, the size of prepared gold nanocups can be easily tuned from tens of nanometers to several micrometers by tuning the diameter of the silica nanospheres. Figures 4a-c show the TEM images of Au nanocups prepared by using silica nanospheres with diameters of 105 nm, 190 nm, and 290 nm, respectively. All the gold nanocups possess excellent morphology, which again proves the success of this method in producing different nanocups. Interestingly, as the initial silica nanospheres become large, the deformable

RF shells can provide more space for the growth of thick nanocups, although the condense time is the same. As shown in Figures 4a-c, the thickness of the Au nanocups increases from 20 nm to 30 nm and 50 nm with the silica diameter largely because of the geometric curvature effect of the initial templates. Small silica nanospheres produce large curvature on the conformal RF layers, which experience large mechanical stress under a similar degree of deformation. The relatively small curvature on large templates instead is easy to deform, thus sustaining the confined growth of thick nanocups.

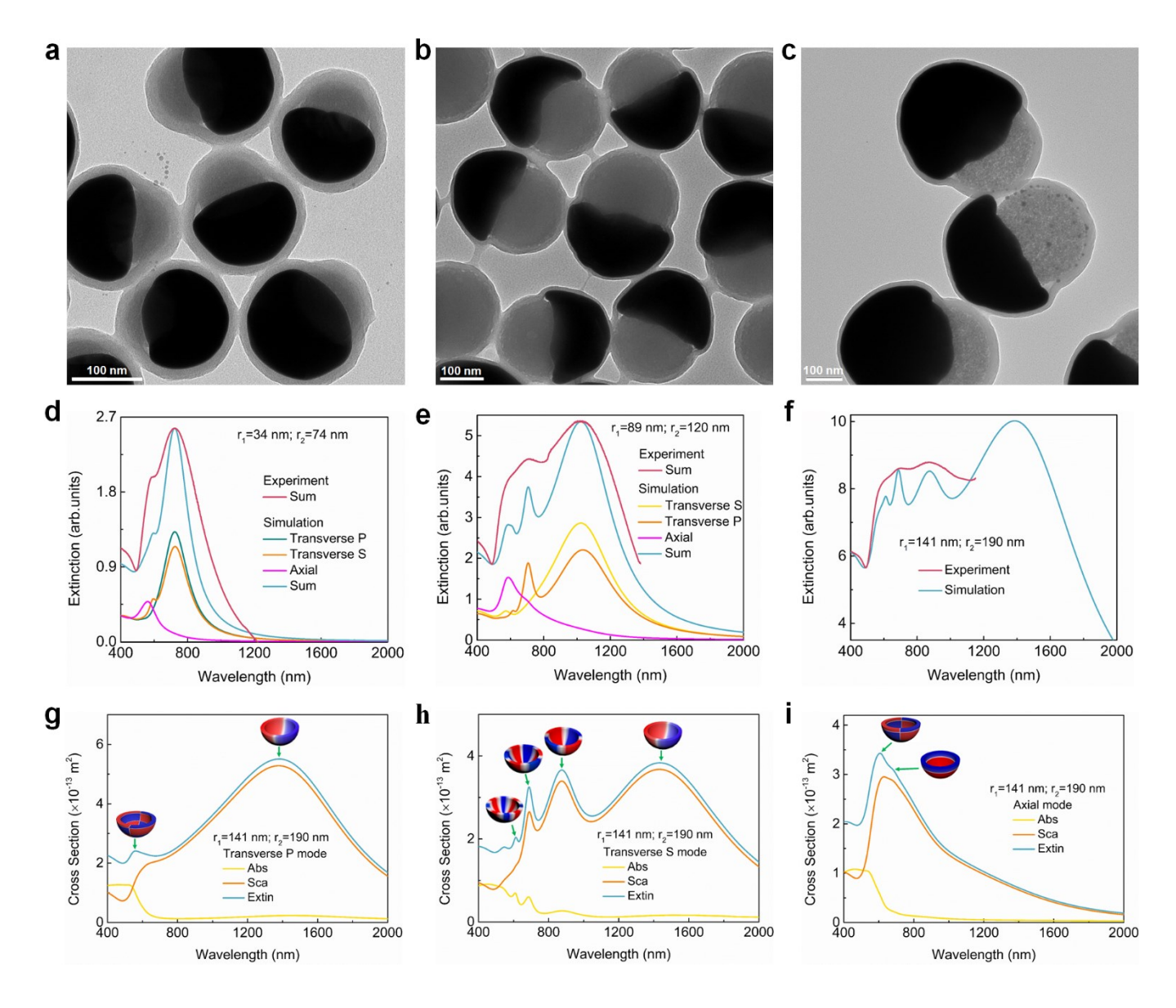


Fig. 4 (a-c) TEM images of SiO₂/Au nanocup@RF with different sizes: (a) $r_1 = 34$ nm, $r_2 = 74$ nm; (b) $r_1 = 89$ nm, $r_2 = 120$ nm; (c) $r_1 = 141$ nm, $r_2 = 290$ nm. (d-f) The corresponding experimental and simulated extinction spectra of the Au nanocups; (g-i) Absorption, scattering and

extinction spectra of gold nanocup with $r_1 = 141$ nm, $r_2 = 290$ nm in three resonance modes. The insets show the schematic diagram of charge distribution at each resonance peak.

Figures 4d-f show the experimental and simulated extinction spectra of Au nanocups corresponding to the products in Figures 4a-c. The inner and outer radius of the gold nanocups are denoted as r_1 and r_2 , respectively. For $r_1=34$, $r_2=74$ nm in Figure 4d, the measured extinction spectrum of Au nanocups have two peaks at 723 nm and 583 nm, which are consistent with the two peaks at 723 nm and 596 nm in simulated spectra. Figure S3a demonstrates the dipolar resonance mode at 723 nm under transverse P excitation. The resonance peak at 561 nm corresponds to the axial mode (Fig.S3b). The transverse S mode has two peaks at 725 nm and 595 nm (Fig.S3c), corresponding to the dipolar and quadrupolar resonance modes, respectively. Notably, the dipolar S mode and dipolar transverse P mode contribute simultaneously to the extinction at 723 nm.

As the size of gold nanocups increases, more plasmon resonance modes and resonance peaks appear. Figure 4e shows the experimental and the simulated spectra for r_1 =89 nm, r_2 =120 nm. Since the size of these nanocups is close to the nanocups in Figure 3, they have similar resonance modes as described above. Compared with small gold nanocups, the spectra of all the resonance modes have noticeable redshifts and become broader. For example, the resonance peaks of small cups (r_1 =34 nm, r_2 =74 nm) at 723 nm and 583 nm shift to 1023 nm and 707 nm, respectively, for large nanocups shown in Figure 4e. The new peak at 587 nm in Figure 4e is ascribed to the superposition of quadrupolar transverse P mode at 573 nm,

hexapolar transverse S mode at 616 nm, and axial mode at 586 nm (Fig.S4). Interestingly, as the size of the nanocup increases, the difference between the dipolar transverse S mode and the dipolar transverse P mode gradually increases, making it easier to distinguish them.

Figure 4f shows the extinction spectra of gold nanocups with the diameter $r_1=141$ nm, $r_2=190$ nm. The simulated extinction spectra have four peaks at 1386, 874, 687, and 611 nm. Figures 4g-4i present the calculated spectra of transverse P mode, transverse S mode, and axial mode, respectively, with their charge distribution showing in the insets. The detailed electric field and charge field simulation results are shown in Figure S5. The resonance wavelengths in transverse mode at 1382 and 560 correspond to the dipolar and hexapolar resonance modes. For transverse S mode, the four prominent peaks at 1434, 875, 688, and 613 nm are the dipolar, quadrupolar, hexapolar and octupolar resonance modes, respectively (Fig.4h). The dipolar resonance at 1434 nm is the symmetric (bonding) plasmon mode, and the other three modes show antisymmetric (antibonding) plasmon modes. The axial resonance mode is similar to that of the nanocup with $r_1=95$, $r_2=130$, located at 607 nm (Fig.4i).

It is worth noting that the plasmon response of the gold nanocups in transverse S modes can be regarded as the interaction of plasmon resonance between the gold nanosphere and the gold nanocavity, which strongly depends on the thickness and the size of the nanocups (Table S1). This interaction produces two types of plasmon resonance: symmetrical plasmon and asymmetrical plasmon. In Figure 3 and Figure 4, for $r_1=34$ nm, $r_2=74 \text{ nm}; r_1=89 \text{ nm}, r_2=120 \text{ nm}, \text{ the plasmon res-}$ onance in the transverse S modes exhibits symmetric plasmon. When $r_1=141$ nm, $r_2=190$ nm, the dipolar resonance in transverse S mode exhibits symmetrical plasmon, while the quadrupolar, hexapolar and octupolar exhibit antisymmetric plasmon. Table S2 shows the resonance wavelengths and modes of the gold nanocups with different sizes in transverse and axial mode. The dipolar modes of both transverse P resonance and the transverse S resonance have the characteristics of strong broadband scattering from visible to near-infrared, which holds great promise in various applications like plasmonic random lasing and optical coherence tomography imaging.

3.4. Plasmonic quantum dot random laser

Random lasers exhibit unique advantages of simple fabrication processes, low fabrication costs, widely tunable emission wavelength, angle-free emission, small size, flexible shape and substrate compatibility [37], which have been extensively investigated in the fields of high-brightness illumination, full-field imaging [38], full-color display, visible-color communications, medical biosensing [39] and integrated devices [40]. Compared with traditional lighting sources, random lasers have two main advantages: laser-level intensity and broad-angular emissions, which show great potential in next-generation illumination. For imaging, random lasers with high photon degeneracy and low spatial coherence

show many advantages like high-quality illumination, directional emission, easy integration, and free of speckles, which are the best in the image quality tests among diverse light sources [38]. However, the output performance of random lasers needs to be further optimized to achieve a low threshold or white light output. The lasing threshold can be affected by scattering characteristics and the concentration of the scatters, the dye concentration, etc. In order to obtain random lasers with superior performance and specific emission wavelength, various gain medium and scattering media have been developed. General gain materials include semiconductor, rare earth-doped active powders, laser dyes, quantum dots, etc. In all types of gain materials, quantum dots have the advantages of size-dependent tunable emission wavelength in broadband spectral region and narrow linewidths, which are an excellent candidate for random lasering. Benefitting from the advantage of the multi-wavelength narrowband emission, quantum dot-based spectrometers have been developed and used in water quality testing [41]. The scatters of random lasers mainly include dielectric scatters and metal nanoparticles. Compared with dielectric scatters, metal nanoparticles of a similar size have a larger scattering cross-section and simultaneous higher gain for light localization from surface plasmon resonance (SPR), which is very beneficial for the preparation of high-performance random lasers with a low threshold. The gold nanocups have strong scattering based on their plasmon resonance. More importantly, the unique multiple plasmon resonance modes of gold nanocups provide strong broadband scattering and large electric field enhancement from the visible to near-infrared spectra region, making it possible to reduce the emission threshold and enhance the feedback loop. Gold nanocups with these properties provide an excellent potential to achieving high-performance plasmonic random laser with low threshold, high efficiency, high Q factor, and multicolor output. Meanwhile, the gold nanocup can realize the change of the incident light from different directions into a single direction, and therefore it is expected to achieve a directional emission plasmon random laser.

To demonstrate the superior optical properties of Au nanocups, we developed a random laser using Au nanocups as an efficient light scatter. Figure 5 (a) schematically illustrates the experimental setup of the plasmonic random laser. The selected Au nanocups have a diameter of ~140 nm and two extinction peaks at 662 nm and 557 nm in water (extinction spectra shown in the inset of Figure 5b and an SEM image shown in Figure S6). CdSe quantum dots with the emission peak at 650 nm, purchased from Beijing Beida Jubang Science & Technology Co., Ltd, were selected as the laser medium. In the experiment, the solution of quantum dots in xylene with different concentrations (30 mg/ml, 40 mg/ml, 50 mg/ml, 60 mg/ml, 70 mg/ml) and the solution of gold nanocups (3 mg/ml) in xylene were mixed at a volume ratio of 5:1, which was then spin-coated into a film on a quartz substrate to make laser device. Figure S7(a) and S7(b) show the SEM images of the surfaces of the films prepared using CdSe solutions with

concentrations of 30 mg/ml and 60 mg/ml. We studied the random laser characteristics of quantum dots with concentrations of 30, 40, 50, 60, and 70 mg/ml. As shown in the emission spectra in Figure S10, the concentration strongly affects the threshold and linewidth. An optimal concentration was determined at 60 mg/ml after considering both threshold and linewidth. We mixed CdSe quantum dots (60 mg/ml) and gold nanocups to form a film for preparing random lasers. Figure 5b shows the extinction spectra of thin films of pure quantum dots and quantum dots doped with gold nanocups. Pure quantum dots film has strong absorption when the wavelength less than 520 nm. For quantum dots doped with gold nanocups, the extinction spectrum shows broadband features centered at 630 nm. The random laser device was pumped by a femtosecond pulse laser with an excitation wavelength of 400 nm, pulse duration of 200 fs, and repetition rate of 1 kHz. Figure 5c shows the photoluminescence (PL) spectrum of pure quantum dots film and the emission spectra of the random laser at different pump energy densities. The PL peak of the CdSe film is located at about 656 nm with an FWHM of about 35 nm. Because the photoluminescence spectrum of CdSe overlaps with the LSPR of Au nanocups, the coupling between PL and plasmon resonance causes Au nanocups to scatter light more effectively, and the radiation from CdSe quantum dots is multiply scattered and amplified by Au nanocups. Meanwhile, the local field enhancement caused by plasmon resonance excitation increases the emission cross section of the quantum dots. For CdSe-doped Au nanocups, at a low pump energy density of $27 \mu J/cm^2$, the emission spectrum exhibited typical broadband emission characteristics with the FWHM of ~35 nm.

When the pump energy density increases to 35 μ J/cm², the emission centers at ~ 646 nm and features an FWHM of 3.5 nm.

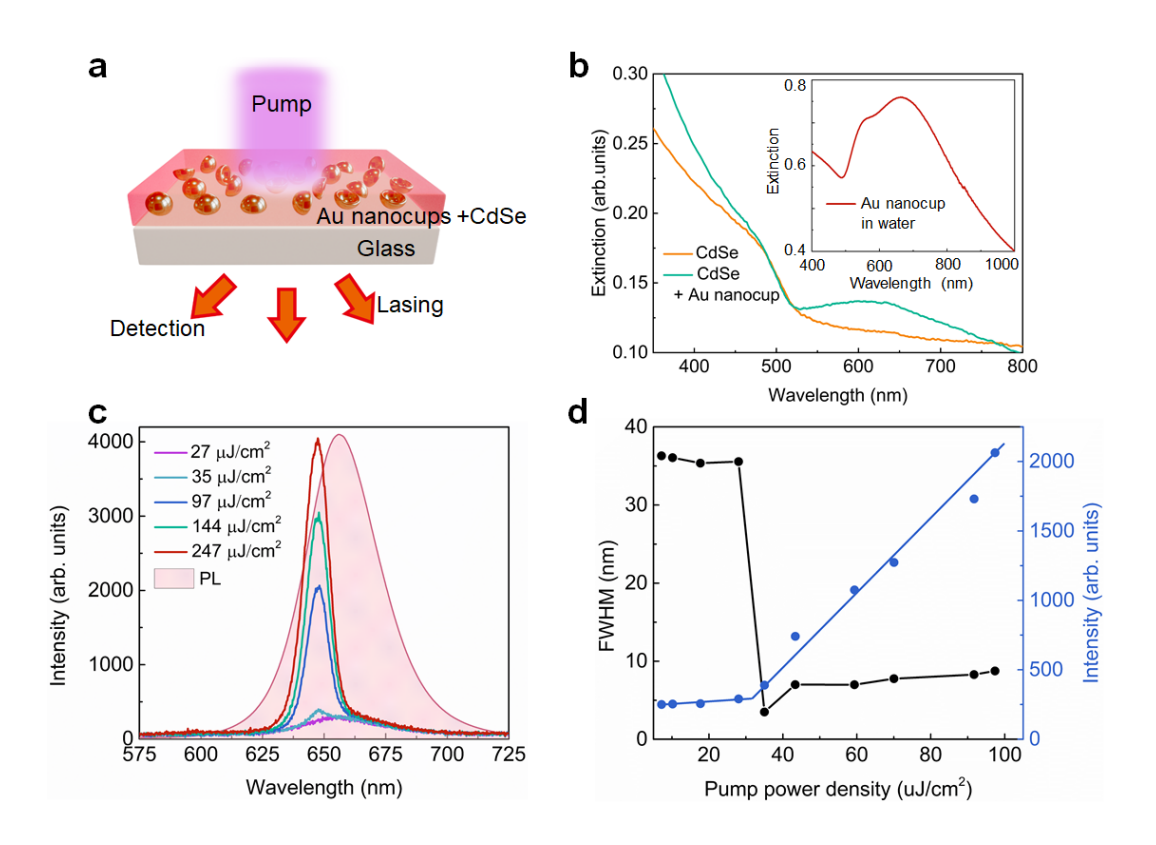


Fig. 5 (a) Schematic of the plasmonic random laser and the laser experimental setup. (b) Extinction spectra of CdSe quantum dot film and CdSe-doped gold nanocup film at a volume ratio of 1 to 5. Inset: the extinction spectrum of gold nanocups in water. (c) Measured PL spectrum of pure quantum dots film and laser emission spectra at different pump energy densities. (d) Output intensity and linewidth of the laser device as a function of the pump energy density.

Figure 5d presents the linewidth and the intensity of the laser spectra as a function of pump energy density, indicating the threshold of the random laser is about $35~\mu J/cm^2$. When the pump energy density reaches the emission threshold, the spectral linewidth dramatically narrowed from 32 to 3.5 nm, demonstrating that laser emission occurred. As the pump energy density increases, the laser emission intensity gradually increases. In order to intuitively illustrate the excellent characteristics of gold nanocups, we compared the performance of quantum dot random lasers of silver

nanospheres, gold nanorods, and gold nanostars [42-44], by considering the scatterer, quantum dots, pump source, threshold, and linewidth as shown in Table S3. Gold nanocups result in the lowest threshold (35 μJ/cm²), again proving their strong scattering characteristics and unique electric field enhancement characteristics. Gold nanocups have strong broadband scattering from their multi-mode plasmon resonance. Meanwhile, most quantum dots can be excited by a single 400-nm pump light. It is highly possible to achieve

multi-wavelength random lasers or white light lasers if the gold nanocups are mixed with multiple quantum dots. This proposed approach is expected to overcome existing challenges in preparing wideband or multi-wavelength random lasers. It is worth noting that gold nanocup can redirect incident light or intracavity emission light in the direction of cup opening that exhibits unidirectional light output[3,4,16], which offers the possibility to realize nanoscale unidirectional random lasing.

4. Conclusions

In summary, we have developed a versatile confined growth method for preparing gold nanocups with controllable morphology and tunable optical properties. It is a simple and ingenious preparation method that uses silica spheres and phenolic shells as deformable templates. This seeded growth method allows the large-scale production of nanocups with various sizes and chemical components. Our experimental studies and simulations confirm numerical that gold nanocups exhibit scattering-dominated optical properties under three typical plasmon excitation modes. Specifically, the transverse S mode has multiple resonance modes, such as dipolar, quadrupolar, and hexapolar, depending on nanocup sizes. Using the strong scattering of the unique Au nanocups, plasmonic quantum dot random laser has been achieved by simply mixing gold nanocups with CdSe quantum dots, which demonstrates high fluorescence feedback and amplification. The fabrication technology and highly tunable LSPR of Au nanocups may have broad applications in the fields of optical nanoantennas,

OCT imaging, photoacoustic imaging, and random lasing.

Conflicts of interest

There are no conflicts to declare.

Acknowledgements

J.Z. and Z.L. contributed equally to this work. This work was supported by the U.S. National Science Foundation (CHE-1808788). J.Z. acknowledges the support from the China Scholarship Council and the National Natural Science Foundation of China (61905016, 61735002). We also thank Chao Chen and Xinping Zhang for their kind help in device testing.

Data Availability

Data supporting the findings of this study are available from the corresponding author on request.

References

- 1. Z. Li, W. Wang, Y. Yin. Colloidal assembly and active tuning of coupled plasmonic nano spheres. Trends in Chemistry. (2020). https://doi.org/https://doi.org/10.1016/j.trechm.202 0.03.008
- 2. N. A. Mirin, N. J. Halas. Light-bending nano particles. Nano Lett. **9**(3) (2009) 1255-1259. https://doi.org/https://doi.org/10.1021/nl900 208z
- 3. N. S. King, M. W. Knight, N. Large, A. M. G oodman, P. Nordlander, N. J. Halas. Orientin g nanoantennas in three dimensions to contro l light scattering across a dielectric interface. Nano Lett. **13**(12) (2013) 5997-6001. https://doi.org/https://doi.org/l0.1021/nl403199z
- 4. Y. Zhang, A. Barhoumi, J. B. Lassiter, N. J. Halas. Orientation-preserving transfer and di rectional light scattering from individual light t-bending nanoparticles. Nano Lett. **11**(4) (2 011) 1838-1844. https://doi.org/https://doi.org/10.1021/nl2008357

- 5. H. Mi, L. Wang, Y. Zhang, G. Zhao, R. Jiang. Control of the emission from electric and ma gnetic dipoles by gold nanocup antennas. Op tics express. 27(10) (2019) 14221-14230. https://doi.org/https://doi.org/10.1364/OE.27.014221
- 6. J. B. Pendry. Negative refraction makes a per fect lens. Phys Rev Lett. **85**(18) (2000) 3966 . https://doi.org/https://doi.org/10.1103/PhysRevLett.85.3966
- 7. J. Yao, Z. Liu, Y. Liu, Y. Wang, C. Sun, G. B artal, A. M. Stacy, X. Zhang. Optical negative refraction in bulk metamaterials of nanowires. Science. **321**(5891) (2008) 930-930. https://doi.org/10.1126/science.1157566
- 8. N. Fang, H. Lee, C. Sun, X. Zhang. Sub-diffr action-limited optical imaging with a silver s uperlens. Science. **308**(5721) (2005) 534-53 7. https://doi.org/10.1126/science.1108759
- 9. M. Khorasaninejad, W. T. Chen, R. C. Devlin, J. Oh, A. Y. Zhu, F. Capasso. Metalenses at visible wavelengths: Diffraction-limited focusing and subwavelength resolution imaging. Science. **352**(6290) (2016) 1190-1194. https://doi.org/10.1126/science.aaf6644
- 10. X. Ni, Z. J. Wong, M. Mrejen, Y. Wang, X. Zhang. An ultrathin invisibility skin cloak for visible light. Science. **349**(6254) (2015) 13 10-1314. https://doi.org/10.1126/science.aac 9411
- 11. Y. Li, S. Kita, P. Muñoz, O. Reshef, D. I. Vu lis, M. Yin, M. Lončar, E. Mazur. On-chip z ero-index metamaterials. Nature Photonics. 9 (11) (2015) 738-742. https://doi.org/10.1038/nphoton.2015.198
- 12. S. Chen, Y. Zhang, T.-M. Shih, W. Yang, S. Hu, X. Hu, J. Li, B. Ren, B. Mao, Z. Yang. P lasmon-induced magnetic resonance enhance d raman spectroscopy. Nano Lett. **18**(4) (201 8) 2209-2216. https://doi.org/https://doi.org/10.1021/acs.nanolett.7b04385
- L. Ma, Y.-L. Chen, X.-P. Song, D.-J. Yang, H.-X. Li, S.-J. Ding, L. Xiong, P.-L. Qin, X.-B. Chen. Structure-adjustable gold nanoing ots with strong plasmon coupling and magne tic resonance for improved photocatalytic activity and sers. ACS Applied Materials & Interfaces. 12(34) (2020) 38554-38562. https://doi.org/10.1021/acsami.0c09684
- 14. M. Cortie, M. Ford. A plasmon-induced curre nt loop in gold semi-shells. Nanotechnology.

- 18(23) (2007) 235704. https://doi.org/https://doi.org/10.1088/0957-4484/18/23/235704
- 15. Z. Li, Y. Yin. Stimuli-responsive optical nan omaterials. Adv Mater. **31**(15) (2019) 18070 61. https://doi.org/https://doi.org/10.1002/adma.201807061
- 16. M. Wang, Y. Yin. Magnetically responsive n anostructures with tunable optical properties. J Am Chem Soc. **138**(20) (2016) 6315-6323 . https://doi.org/https://doi.org/10.1021/jacs.6b02346
- 17. Z. Li, Z. Ye, L. Han, Q. Fan, C. Wu, D. Ding , H. L. Xin, N. V. Myung, Y. Yin. Polarizati on-modulated multidirectional photothermal actuators. Adv Mater. **33**(3) (2021) 2006367. https://doi.org/https://doi.org/10.1002/adma.202006367
- 18. N. S. King, Y. Li, C. Ayala-Orozco, T. Bran nan, P. Nordlander, N. J. Halas. Angle-and s pectral-dependent light scattering from plas monic nanocups. Acs Nano. **5**(9) (2011) 725 4-7262. https://doi.org/https://doi.org/10.1021/nn202086u
- 19. A. Gao, W. Xu, Y. Ponce de León, Y. Bai, M. Gong, K. Xie, B. H. Park, Y. Yin. Controlla ble fabrication of au nanocups by confined-s pace thermal dewetting for oct imaging. Adv. Mater. **29**(26) (2017) 1701070. https://doi.org/10.1002/adma.201701070
- F. Gao, M. Sun, L. Xu, L. Liu, H. Kuang, C. Xu. Biocompatible cup-shaped nanocrystal with ultrahigh photothermal efficiency as tu mor therapeutic agent. Adv Funct Mater. 27(24) (2017) 1700605. https://doi.org/https://doi.org/10.1002/adfm.201700605
- 21. R. Jiang, F. Qin, Y. Liu, X. Y. Ling, J. Guo, M. Tang, S. Cheng, J. Wang. Colloidal gold nanocups with orientation-dependent plasmo nic properties. Adv Mater. **28**(30) (2016) 63 22-6331. https://doi.org/https://doi.org/10.10 02/adma.201601442
- 22. X. Li, H. Hu, D. Li, Z. Shen, Q. Xiong, S. Li, H. J. Fan. Ordered array of gold semishells on tio2 spheres: An ultrasensitive and recycl able sers substrate. ACS applied materials & interfaces. 4(4) (2012) 2180-2185. https://doi.org/10.1021/am300189n
- 23. Y. Zhang, N. K. Grady, C. Ayala-Orozco, N. J. Halas. Three-dimensional nanostructures as highly efficient generators of second harm onic light. Nano Lett. **11**(12) (2011) 5519-55 23. https://doi.org/https://doi.org/10.1021/nl2033602

- 24. S.-J. Ding, H. Zhang, D.-J. Yang, Y.-H. Qiu, F. Nan, Z.-J. Yang, J. Wang, Q.-Q. Wang, H.-Q. Lin. Magnetic plasmon-enhanced secon d-harmonic generation on colloidal gold nan ocups. Nano Lett. **19**(3) (2019) 2005-2011. https://doi.org/https://doi.org/10.1021/acs.nan olett.9b00020
- 25. P. Van Dorpe, J. Ye. Semishells: Versatile pl asmonic nanoparticles. ACS nano. **5**(9) (201 1) 6774-6778. https://doi.org/https://doi.org/10.1021/nn203142k
- 26. R. Drevinskas, T. Rakickas, A. Selskis, L. R osa, R. n. Valiokas. Cup-shaped nanoantenn a arrays for zeptoliter volume biochemistry a nd plasmonic sensing in the visible waveleng th range. ACS applied materials & interfaces . 9(22) (2017) 19082-19091. https://doi.org/10.1021/acsami.7b02749
- 27. M. Kovylina, N. Alayo, A. Conde-Rubio, X. Borrisé, G. Hibbard, A. Labarta, X. Batlle, F. Pérez-Murano. Au cylindrical nanocup: A g eometrically, tunable optical nanoresonator. Appl Phys Lett. **107**(3) (2015) 033102. https://doi.org/10.1063/1.4927053
- 28. X. Li, Y. Shang, J. Lin, A. Li, X. Wang, B. Li, L. Guo. Temperature-induced stacking to create cu2o concave sphere for light trapping capable of ultrasensitive single-particle surface-enhanced raman scattering. Adv Funct Mater. 28(33) (2018) 1801868. https://doi.org/10.1002/adfm.201801868
- 29. J. C. Love, B. D. Gates, D. B. Wolfe, K. E. P aul, G. M. Whitesides. Fabrication and wetti ng properties of metallic half-shells with sub micron diameters. Nano Lett. **2**(8) (2002) 89 1-894. https://doi.org/https://doi.org/10.1021/nl0256331
- 30. W. Stöber, A. Fink, E. Bohn. Controlled gro wth of monodisperse silica spheres in the mi cron size range. J Colloid Interface Sci. **26**(1) (1968) 62-69. https://doi.org/https://doi.org/10.1016/0021-9797(68)90272-5
- 31. Q. Zhang, T. Zhang, J. Ge, Y. Yin. Permeabl e silica shell through surface-protected etching. Nano Lett. **8**(9) (2008) 2867-2871. https://doi.org/https://doi.org/10.1021/nl8016187
- 32. Z. Li, J. Jin, F. Yang, N. Song, Y. Yin. Coup ling magnetic and plasmonic anisotropy in h ybrid nanorods for mechanochromic respons es. Nature communications. **11**(1) (2020) 1-1 1. https://doi.org/https://doi.org/10.1038/s41467-020-16678-8

- 33. N. Li, Q. Zhang, J. Liu, J. Joo, A. Lee, Y. Gan, Y. Yin. Sol–gel coating of inorganic nano structures with resorcinol–formaldehyde resin. Chem Commun. **49**(45) (2013) 5135-5137. https://doi.org/https://doi.org/10.1039/C3CC41456F
- 34. Z. Li, Q. Fan, C. Wu, Y. Li, C. Cheng, Y. Yi n. Magnetically tunable plasmon coupling of au nanoshells enabled by space-free confine d growth. Nano Lett. **20**(11) (2020) 8242-82 49. https://doi.org/https://doi.org/10.1021/acs.nanolett.0c03350
- 35. E. Prodan, C. Radloff, N. J. Halas, P. Nordla nder. A hybridization model for the plasmon response of complex nanostructures. science . **302**(5644) (2003) 419-422. https://doi.org/10.1126/science.1089171
- 36. J. Rodríguez-Fernández, J. Pérez-Juste, F. J. García de Abajo, L. M. Liz-Marzán. Seeded growth of submicron au colloids with quadru pole plasmon resonance modes. Langmuir. **2 2**(16) (2006) 7007-7010. https://doi.org/10.1021/la060990n
- 37. H. Cao. Random lasers: Development, featur es and applications. Optics and photonics ne ws. **16**(1) (2005) 24-29. https://doi.org/10.1364/OPN.16.1.000024
- 38. B. Redding, M. A. Choma, H. Cao. Speckle-free laser imaging using random laser illumi nation. Nature photonics. **6**(6) (2012) 355-35 9. https://doi.org/https://doi.org/10.1038/nph oton.2012.90
- 39. R. C. Polson, Z. V. Vardeny. Random lasing in human tissues. Appl Phys Lett. **85**(7) (20 04) 1289-1291. https://doi.org/https://doi.org/10.1063/1.1782259
- 40. S.-W. Chang, W.-C. Liao, Y.-M. Liao, H.-I. Lin, H.-Y. Lin, W.-J. Lin, S.-Y. Lin, P. Peru mal, G. Haider, C.-T. Tai. A white random la ser. Scientific reports. **8**(1) (2018) 1-10. https://doi.org/10.1038/s41598-018-21228-w
- 41. J. Bao, M. G. Bawendi. A colloidal quantum dot spectrometer. Nature. **523**(7558) (2015) 67-70. https://doi.org/https://doi.org/10.1038/nature14576
- 42. F. Shan, X.-Y. Zhang, J.-Y. Wu, T. Zhang. H ot spots enriched plasmonic nanostructure-in duced random lasing of quantum dots thin fil m. Chinese Physics B. 27(4) (2018) 047804. https://doi.org/https://doi.org/10.1088/1674-1056/27/4/047804

- 43. J. Tong, X. Shi, L. Niu, X. Zhang, C. Chen, L. Han, S. Zhang, T. Zhai. Dual-color plasmo nic random lasers for speckle-free imaging. Nanotechnology. 31(46) (2020) 465204. https://doi.org/https://doi.org/10.1088/1361-6528/abaadc
- 44. Z. Xu, H. Zhang, C. Chen, G. Aziz, J. Zhang, X. Zhang, J. Deng, T. Zhai, X. Zhang. A sili con-based quantum dot random laser. RSC A dv. 9(49) (2019) 28642-28647. https://doi.org/10.1039/C9RA04650J